neuroblastomas demonstrated good outcomes (GGW1s: 100%, $n=5$; GGW2s: 100%, $n=2$; GGW3s: 100%, $n=11$; GGW4s: 97%, $n=91$ and GGW5s: 89%, $n=18$). The intermediate 5-year cumulative survival rates were demonstrated in GGPs tumors (GGP1s: 80%, $n=6$; GGP2s: 57%, $n=7$; GGP3s: 75%, $n=26$

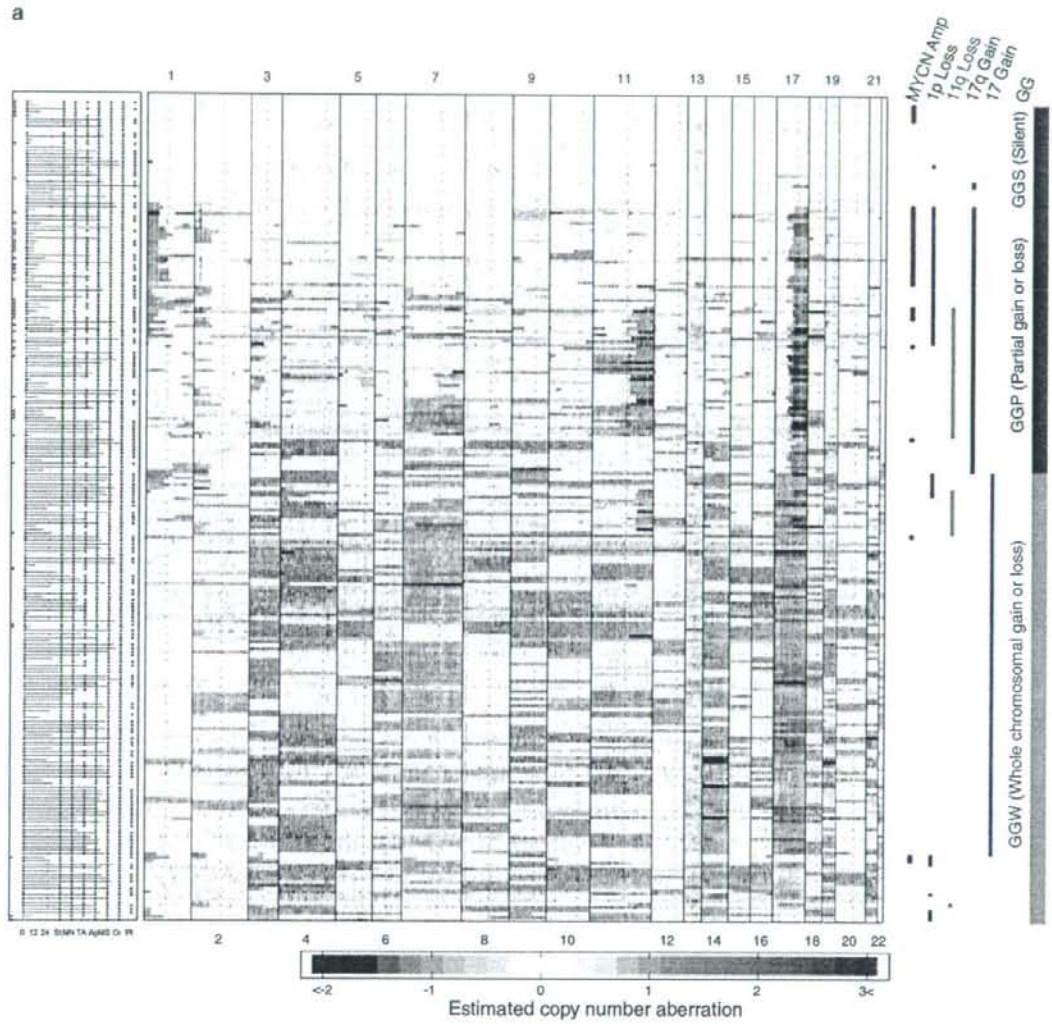

Figure 1 Genomic signatures of 236 primary neuroblastomas by array-based comparative genomic hybridization (array-CGH). (**a**) Overall schematic of the genomic signatures of 236 primary neuroblastomas. The left panel summarizes information about patient diagnostic factors: survival time in months after diagnosis for censored (blue bars) or dead (red bars) patients, stages 1, 2 and 4 s (blue) or 3 and 4 (red) (ST), *MYCN* amplification (red) or not (blue) (MN), TrkA low (red) or high expression (blue) (TA), age more (red) or less (blue) than 12 months (Ag), sporadic tumors (red) or tumors detected by mass screening (blue) (Ms), adrenal gland (red) or others (blue) in origin (Or) and hyperploidy (blue) or diploidy/tetraploidy (red) (Pl). The central panel shows estimated copy number aberrations of DNA as color matrixes (blue: loss, red: gain) at chromosome locations complementary to BAC clones in each sample. The right panel shows the important features of chromosomal events, including *MYCN* amplification, deletions of chromosomes 1p and 11q, chromosome 17q gain and whole chromosome 17 gain. Furthermore, genomic groups (GGS, silent genomic group; GGP, partial chromosomal gains/losses genomic group and GGW, whole gains and/or losses genomic group) are also indicated. (**b**) Genomic signatures in each genomic group and the 5-year survival rates for all neuroblastomas including MS detected and sporadic tumors. Regarding each genomic group, the colored histogram represents the rates of gains and losses for each clone, where the red areas on the baseline correspond to gain and the blue areas under the baseline to loss. The right panel indicates the presence of *MYCN* amplification, 1p loss, 11q loss, 17q gain and 17 gain. The 5-year survival rates (SR) of each genomic subgroup are indicated in the right panel.

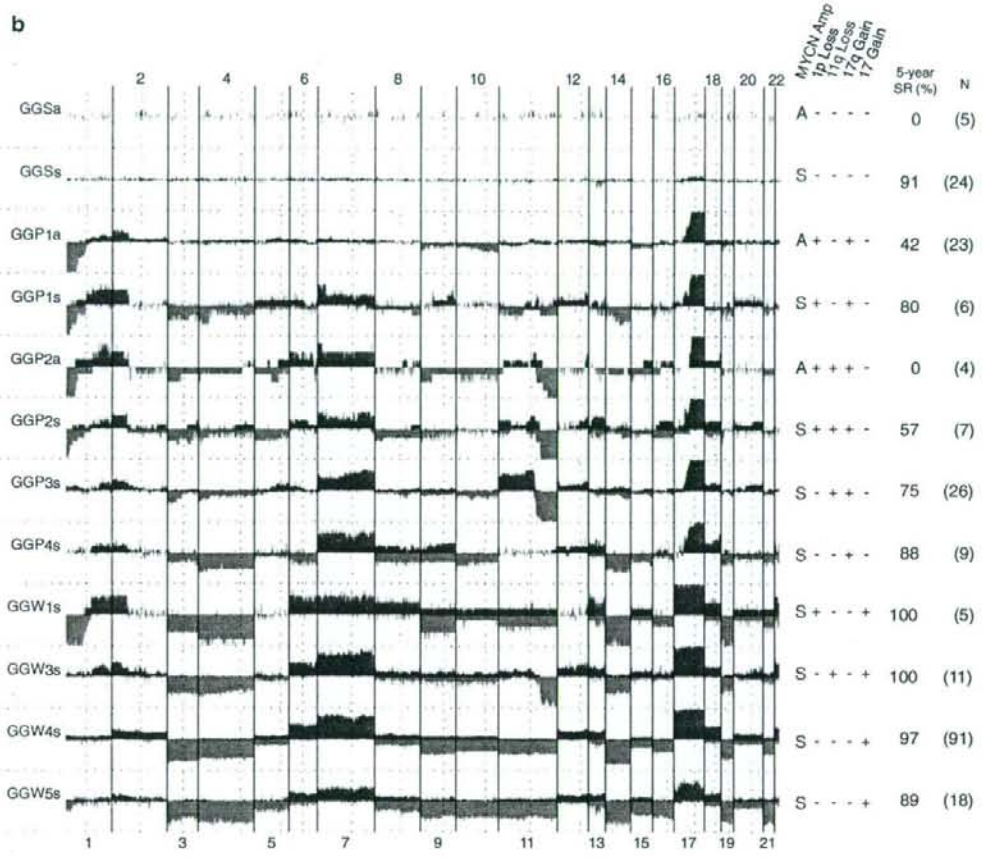

Figure 1 Continued.

and GGP4s: 88%, $n=9$). Interestingly, in GGPs tumors, 1p loss (GGP1s, $n=6$) and 11q loss (GGP3s, $n=26$) seemed to have a similar effect on patient prognosis (5-year survival rates: 80 and 75%, respectively). However, GGP2s tumors with both 1p loss and 11q loss ($n=7$) had a poorer prognosis (57%) in an additive manner. Furthermore, the addition of 11q loss and 1q gain to *MYCN* amplification apparently afforded absolutely poor outcomes as suggested by the comparison between GGP1a (42%) and GGP2a tumors (0%). An analysis of 112 sporadic tumors also revealed a similar tendency except GGP1s, in which 2 sporadic tumors showed 0% survival, whereas all 4 MS-detected tumors gave good outcomes (Table 1 and Supplementary Figure S3). These suggested that *MYCN* amplification had the most powerful influence on clinical outcomes. We next compared the patterns of whole genome abnormalities of *MYCN*-amplified neuroblastomas between survivors (disease-free for more than 2 years after initiating treatment) and non-survivors (dead of disease). One of the most striking differences was frequent loss of 11q (Supplementary Figure S4).

Effects of genomic signatures, MYCN amplification and age on prognosis in sporadic neuroblastomas

Figure 2 shows the Kaplan–Meier cumulative survival curves in each genetic group. In sporadic neuroblastomas, the overall survival rates of GGW, GGS and GGP were 80% ($n=36$), 68% ($n=23$) and 43% ($n=53$), respectively (Figure 2a). The prognosis of GGP was significantly poorer than that of GGW ($P=0.002$). In MS-detected tumors, on the other hand, the survival rates of GGW, GGS and GGP were 100% ($n=94$), 100% ($n=6$) and 96% ($n=24$), respectively (no significant difference among the groups; Figure 2b). The main difference between sporadic and MS-detected tumors was that the latter was detected before 1 year of age and had very few *MYCN* amplifications. Therefore, sporadic tumors were next subcategorized according

to the presence or absence of *MYCN* amplification. Figure 3a shows that the 5-year survival rates of patients with GGSs ($n=18$), GGWs ($n=33$) and GGPs ($n=25$) tumors were 89, 85 and 53%, respectively, whereas those of patients with GGSa ($n=5$), GGWa ($n=3$) and GGPa ($n=28$) tumors involving *MYCN* amplification were 0, 33 and 34%, respectively (Figure 3b). We then further examined the survival curves of patients with *MYCN*-nonamplified tumors in young (<1-year-old) and old (≥1-year-old) patients. Figure 3c shows the 5-year survival rates of 88, 86 and 67% in GGWs ($n=24$), GGSs ($n=7$) and GGPs ($n=3$) tumors, respectively, among young patients, whereas they were 76, 91 and 51% in GGWs ($n=9$), GGSs ($n=11$) and GGPs ($n=22$) tumors, respectively, among old patients (Figure 3d). The former pattern was similar to that in MS-detected tumors, which had high percentages of GGW tumors, whereas the latter contained high incidences of GGP tumors.

Table 1 Five-year overall survival rates of the patients with each genomic subgroup of sporadic neuroblastomas

	N	*5-Year OS (%)*
GGS		
GGSa	5	0
GGSs	18	89
GGP		
GGP1a	22	44
GGP1s	2	0
GGP2a	4	0
GGP2s	5	40
GGP3a	1	0
GGP3s	15	59
GGP4a	1	0
GGP4s	3	67
GGW		
GGW1a	0	—
GGW1s	0	—
GGW2a	0	—
GGW2s	1	100
GGW3a	0	—
GGW3s	3	100
GGW4a	1	0
GGW4s	23	87
GGW5a	2	50
GGW5s	6	67

Abbreviations: GGP, partial chromosomal gains/losses genomic group; GGS, silent genomic group; GGW, whole gains and/or losses genomic group; OS, overall survival rate.

Segregation of the prognosis of sporadic neuroblastomas with a single copy of MYCN by genomic and molecular signatures

Recently, we have generated a clinically useful cDNA microarray carrying 200 genes that predicts the prognosis of neuroblastomas with an accuracy rate of 89% (Ohira *et al*., 2005). The univariate analysis of 112 sporadic neuroblastomas showed that both genomic signatures (GGP vs GGW+GGS, $P=0.003$) and molecular signatures (posterior value<0.5 vs ≥0.5, $P<0.001$) were highly significant prognostic indicators, like other variables including age ($P=0.006$), stage ($P<0.001$), tumor origin ($P=0.001$), *TrkA* expression ($P=0.004$), Shimada classification ($P<0.001$) and *MYCN* amplification ($P<0.001$; Table 2). In addition, genomic signature was a prognostic factor independent from molecular signature, age and tumor origin, although it showed no prognostic significance when stage, Shimada classification, or *MYCN* amplification was controlled (Table 2). Even in sporadic neuroblastomas with a single copy of *MYCN*, the highest significance according to the univariate analysis was given to molecular signature ($P=0.002$), followed by tumor origin ($P=0.006$) and genomic signature ($P=0.010$; Table 2). The multivariate analysis also showed that genomic signature was a prognostic indicator independent from molecular signature or tumor origin (Table 2). As shown in Figure 4, our in-house expression microarrays segregated the survival curves of patients with sporadic tumors lacking *MYCN* amplification (GGSs+GGPs+GGWs) into the favorable (94%, $n=17$) and unfavorable (42%, $n=13$) prognosis groups ($P=0.001$).

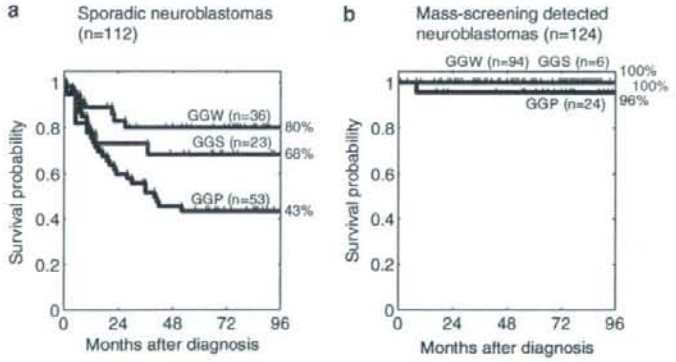

Figure 2 Kaplan Meier survival curves in three genomic groups (GGS, GGP and GGW) based on array-CGH. (a) Sporadic neuroblastomas: GGS vs GGP: $P=0.109$, GGS vs GGW: $P=0.320$ and GGP vs GGW: $P=0.002$. (b) Mass screening-detected neuroblastomas: GGS vs GGP: $P=1.000$, GGS vs GGW: $P=1.000$ and GGP vs GGW: $P=1.000$.

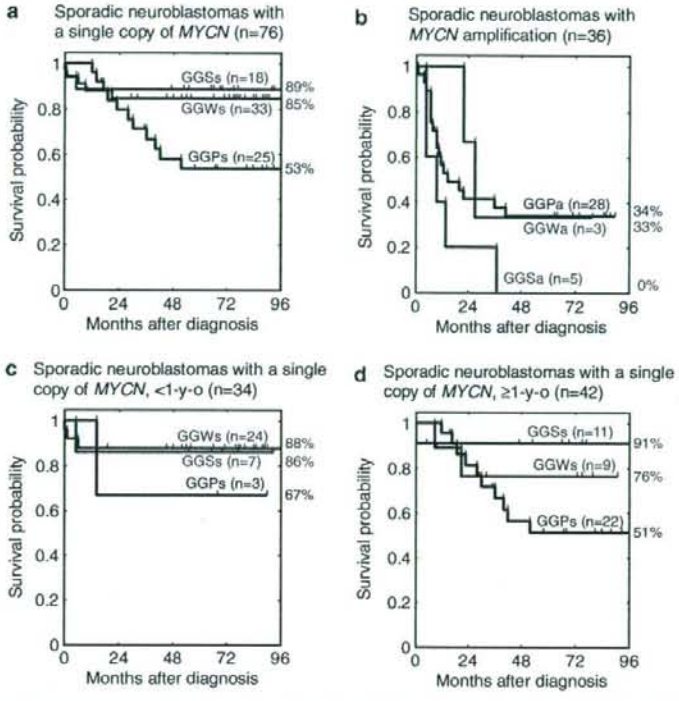

Figure 3 Kaplan Meier survival curves in three genomic groups (GGS, GGP and GGW) of sporadic neuroblastomas based on array-CGH. (**a**) Sporadic neuroblastomas with a single copy of *MYCN* GGS vs GGP: $P=0.035$, GGS vs GGW: $P=0.736$ and GGP vs GGW: $P=0.033$. (**b**) Sporadic neuroblastomas with *MYCN* amplification GGS vs GGP: $P=0.104$, GGS vs GGW: $P=0.156$ and GGP vs GGW: $P=0.642$. (**c**) Sporadic neuroblastomas with a single copy of *MYCN* in patients under 1 year of age GGS vs GGP: $P=1.000$, GGS vs GGW: $P=0.919$ and GGP vs GGW: $P=0.412$. (**d**) Sporadic neuroblastomas with a single copy of *MYCN* in patients over 1 year of age. GGS vs GGP: $P=0.063$, GGS vs GGW: $P=0.478$ and GGP vs GGW: $P=0.481$.

Discussion

The present array-CGH analysis revealed the whole feature of the genomic abnormality patterns of sporadic and MS-detected neuroblastomas. The patterns of genomic aberrations in MS-detected neuroblastomas are similar to those in sporadic tumors, suggesting that they are genetically genuine neuroblastomas which are similar to sporadic tumors found in patients under 1 year of age. Indeed, both of them have a high tendency to regress spontaneously. The exceptions we found are that the incidence of GGPs tumors is relatively higher in MS-detected tumors than in sporadic tumors found among young patients and that their clinical outcome is very good.

BAC array-based aCGH analyses have defined several minimal critical regions of gains and losses in 1p, 2p and 11q. These included minimal losses in 10 Mb regions of 1p36.3 (1pter to RP11-199O1, *D1S244*) and 11q23 (from RP11-42L18 to RP11-45N4). The 2 Mb region in 1p36.2–36.3 detected by a BAC clone RP11-219F4 (*D1S507*) exhibited highest deletion frequency of 32%. By combining the expression data obtained by the in-house microarrays harboring approximately 5340 genes derived from primary neuroblastomas, several candidate genes including *CHD5* at 1p36 (Bagchi *et al.*, 2007) as well as *Survivin* at 17q25 (Islam *et al.*, 2000) were identified as lowly and highly expressed genes in neuroblastomas with advanced stages, respectively (manuscript in preparation). The amplicon surrounding the *MYCN* locus was ranged from 2.4 Mb proximal (*G14110*) to 5 Mb distal (*D2S387*) of *MYCN* itself and gains were further extended to wider range, from 2pter to 2p11.

To date, the presence of the GGS subgroup with very silent aberrations of the tumor genome has never been verified definitely. The distribution of GGS tumors is very unique; namely, they are present in both MS detected and sporadic tumors removed from the patients under 1 year of age. They are also found in tumors obtained from the patients over 1 year of age, and some of them possess *MYCN* amplification. Furthermore, GGS tumors mostly show diploid karyotype. These facts suggest that GGSs tumors might represent neuroblastoma at an early stage of carcinogenesis with early oncogenic hit(s), which later develop to GGP or

Table 2 Univariate and multivariate analyses of genomic and molecular signature as well as other prognostic factors in sporadic neuroblastomas

	Sporadic NBLs (all cases)				*Sporadic NBLs (MYCN, single copy)*			
	N	P	*HR*	*CI*	N	P	*HR*	*CI*
Genomic signature (GGP vs GGW + GGS)	53 vs 59	0.003	2.59	(1.36, 4.90)	25 vs 51	0.010	3.41	(1.32, 8.82)
Molecular signature (posterior <0.5 vs $\geqslant 0.5$)	22 vs 18	<0.001	11.15	(2.52, 49.35)	13 vs 17	0.002	14.05	(1.72, 114.89)
Age ($\geqslant$ 1-year old vs $<$ 1-year old)	74 vs 38	0.006	2.67	(1.24, 5.77)	42 vs 34	0.070	2.47	(0.88, 6.96)
Stage (3, 4 vs 1, 2, 4s)	73 vs 38	<0.001	4.92	(1.93, 12.54)	38 vs 37	0.038	2.80	(1.00, 7.88)
Origin (adrenal vs nonadrenal)	72 vs 40	0.001	3.22	(1.43, 7.25)	41 vs 35	0.006	4.59	(1.33, 15.85)
TRKA expression (low vs high)	52 vs 36	0.004	3.37	(1.36, 8.34)	24 vs 36	0.766	1.21	(0.34, 4.31)
Shimada (unfavorable vs favorable)	39 vs 37	<0.001	4.54	(1.71, 12.07)	14 vs 36	0.668	1.37	(0.33, 5.75)
MYCN (amplification vs single copy)	36 vs 75	<0.001	3.98	(2.16, 7.35)	—	—	—	—
Genomic signature (GGP vs GGW + GGS)	15 vs 25	0.045	2.89	(1.01, 8.30)	8 vs 22	0.031	5.46	(1.09, 27.40)
Molecular signature (posterior <0.5 vs $\geqslant 0.5$)	22 vs 18	0.002	7.52	(1.69, 33.38)	13 vs 17	0.034	7.41	(0.90, 60.87)
Genomic signature (GGP vs GGW + GGS)	53 vs 59	0.048	1.99	(1.05, 3.78)	25 vs 51	0.055	2.85	(1.10, 7.36)
Age ($\geqslant$ 1-year old vs $<$ 1-year old)	74 vs 38	0.132	1.88	(0.87, 4.06)	42 vs 34	0.549	1.44	(0.51, 4.05)
Genomic signature (GGP vs GGW + GGS)	53 vs 58	0.416	1.34	(0.71, 2.54)	25 vs 50	0.098	2.61	(1.01, 6.76)
Stage (3, 4 vs 1, 2, 4s)	73 vs 38	0.005	4.06	(1.60, 10.34)	38 vs 37	0.496	1.56	(0.56, 4.40)
Genomic signature (GGP vs GGW + GGS)	53 vs 59	0.012	2.23	(1.18, 4.23)	25 vs 51	0.015	3.19	(1.23, 8.26)
Origin (adrenal vs non-adrenal)	72 vs 40	0.006	2.78	(1.24, 6.26)	41 vs 35	0.008	4.30	(1.24, 14.88)
Genomic signature (GGP vs GGW + GGS)	41 vs 47	0.079	2.17	(0.96, 4.95)	18 vs 42	0.050	3.75	(1.06, 13.33)
TRKA expression (low vs high)	52 vs 36	0.078	2.34	(0.95, 5.79)	24 vs 36	0.727	0.79	(0.22, 2.80)
Genomic signature (GGP vs GGW + GGS)	53 vs 58	0.236	1.53	(0.81, 2.90)	—	—	—	—
MYCN (amplification vs single copy)	36 vs 75	<0.001	3.30	(1.79, 6.08)	—	—	—	—

Abbreviations: CI, confidence interval; GGP, partial chromosomal gains/losses genomic group; GGS, silent genomic group; GGW, whole gains and/or losses genomic group; HR, hazard ratio; *N*, sample number; NBLs, neuroblastomas; *P*, *P*-value.

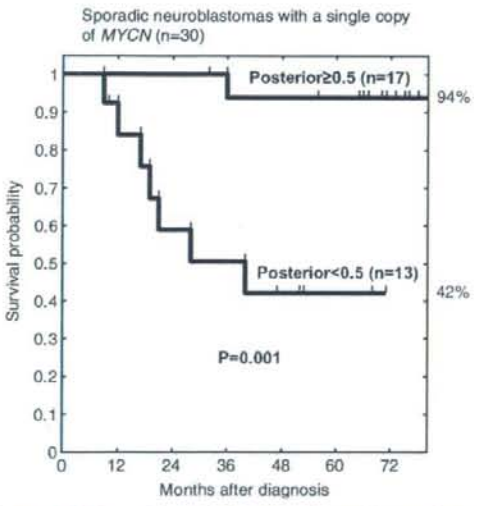

Figure 4 Kaplan Meier survival curves of sporadic neuroblastomas with a single copy of *MYCN* according to the molecular signature. Gene-expression profiling segregated patients into the favorable (posterior score $\geqslant 0.5$) and unfavorable (posterior score <0.5) prognosis groups ($P = 0.001$). The posterior score denotes how likely the patient would show good outcome after 5 years (Ohira *et al*., 2005).

GGW tumors. Since MS did not decrease the incidence of sporadic neuroblastomas (Brodeur *et al*., 2001; Levy, 2005), GGSs tumors in young and old patients might be derived from different progenitor cells. It is interesting that the clinical outcome is very good for patients with *MYCN*-nonamplified GGSs tumors, whereas it is very bad for patients with GGSa tumors possessing *MYCN* amplification, implying again remarkable impact of *MYCN* amplification on the patient's outcome.

The GGP group is characterized by the presence of 17q gain with other chromosomal abnormalities including *MYCN* amplification, 1p loss and 11q loss. Since this group of tumors shows multiple chromosomal aberrations with partial gains and/or losses, unknown causes to induce genomic instability might have triggered genesis of neuroblastoma in progenitor or stem cells of sympathetic cell lineage (Maris and Matthay, 1999; Nakagawara, 2004). The frequently observed GGP tumors are as follows: GGP1a tumors with both 1p loss and *MYCN* amplification and GGP3s tumors with 11q loss but without *MYCN* amplification. The former may belong to a typical *MYCN*-amplified neuroblastoma (White *et al*., 1995) with a 5-year cumulative survival rate of 42% in our series, whereas the latter to the so-called intermediate type tumor (Srivatsan *et al*., 1993; Attiyeh *et al*., 2005) with the rate of 75%. In GGP tumors, it is obvious that *MYCN* amplification has the most powerful impact on the patient prognosis. Interestingly, among the GGPs tumors lacking *MYCN* amplification, 1p loss and 11q loss seem to similarly affect the prognosis. However, GGP2s tumors with both 1p loss and 11q loss show poorer prognosis in an additive manner. The similar additive effect has also been observed in GGP1a (42%

survival) and GGP2a (0% survival) with *MYCN*-amplified tumors. These suggest that 1p loss and 11q loss may independently affect the outcomes of neuroblastoma. Interestingly, one of the main characteristics of the *MYCN*-amplified tumors found in the long-term survivors is a lack of 11q loss (Supplementary Figure S4), corresponding to the observation that the high percentage of 5-year survival rate is shown in the GGP1a group with 1p loss but without 11q loss.

GGW neuroblastoma has a favorable prognosis, as reported (Vandesompele *et al.*, 1998). Since the pattern of chromosomal aberrations is represented by whole chromosomal gains and/or losses, mitotic dysfunction during the cell division cycle in progenitor or stem cells might have generated neuroblastoma (Maris and Matthay, 1999; Nakagawara, 2004). Interestingly, 1p loss or 11q loss in a minor population of GGWs tumors (GGW1s and GGW3s) seems not to affect the prognosis.

The presence of different patterns of genomic aberrations like GGS, GGP and GGW may reflect differences in stem or progenitor cells targeted to generate different genetic subsets of neuroblastomas. Although carcinogenic events to cause neuroblastomas may occur sequentially (Tonini, 1993), our serial analyses of six paired primary and recurrent tumors interestingly suggest that the major genetic events, for example, *MYCN* amplification, 1p loss, 11q loss and 17q gain, could occur not always in order during tumor progression (Supplementary Table S3).

Thus, the genomic signatures presented here successfully categorized new prognostic subgroups of neuroblastomas. The rather consistent patterns of genomic abnormalities provide reliable information to understanding of the genetic bases which underlie the clinical phenotypes of neuroblastomas with different survival rates. However, the pattern of genomic abnormalities may often lack biological significance affecting the clinical behavior of individual tumors. The gene-expression profile well reflects the biology of individual tumor. Therefore, establishment of the combined system of both genomic and molecular signatures is ideal for predicting the prognosis of individual patients with neuroblastoma. The present study has clearly shown that genomic and molecular signatures are independent prognostic indicators and suggests that an expression microarray could compensate for the relevant lack when used only genomic signature. In conclusion, combined genomic and molecular signatures may be clinically useful for constituting an ideal system to categorize and even individualize each tumor, which may make tailored medicine of neuroblastoma possible.

Materials and methods

Patients, tissue specimens and DNA/RNA resources

Tumor specimens were collected from 236 patients who had undergone biopsy or surgery at various institutions in Japan (see Supplementary Information). They included 112 sporadic and 124 MS-detected neuroblastoma specimens. All tumors were histopathologically diagnosed as neuroblastoma or ganglioneuroblastoma and were staged according to the International Neuroblastoma Staging System (Brodeur *et al.*, 1993). Informed consent was obtained at each institution or hospital. The procedure of this study was approved by the Institutional Review Board of the Chiba Cancer Center (CCC7817). Patients were treated by the standard protocols (Kaneko *et al.*, 2002; Iehara *et al.*, 2006) in Japan between 1995 and 2003. All MS-detected tumors were diagnosed between 6 and 8 months after birth by measuring urinary catecholamine metabolites in Japan (Sawada *et al.*, 1984). Fresh neuroblastoma tissues removed during surgery were stored at −80°C. *MYCN* copy number, *TrkA* mRNA expression and DNA ploidy were measured as reported previously (Islam *et al.*, 2000).

Microarray-based comparative genomic hybridization

A chip carrying 2464 BAC clones prepared by ligation-mediated PCR, which covers the whole human genome at roughly 1.2-Mb resolution (Snijders *et al.*, 2001; Albertson *et al.*, 2003), was used. The 500-ng aliquots of tumors and reference DNAs were labeled by random priming with each Cy3-dCTP and Cy5-dCTP (Amersham Pharmacia, Piscataway, NJ, USA). Hybridization was performed as previously reported (Pinkel *et al.*, 1998). UCSF Spot and UCSF Sproc programs to analyse values for spotted clones (Jain *et al.*, 2002) were used. All array-CGH data are available at NCBI Gene Expression Omnibus (GEO, http://www.ncbi.nlm.nih.gov/geo/) with accession number GSE 5784.

cDNA microarrays

In-house cDNA microarrays, carrying 5340 cDNAs obtained from the oligo-capping cDNA libraries generated from anonymous neuroblastoma tissues (Ohira *et al.*, 2003, 2005), were used. Preparation of RNA, hybridization, reading of spots and statistical analyses were conducted as reported previously (Ohira *et al.*, 2005). Gene-expression profile data described in this study is available at NCBI GEO with accession number GSE 5779.

Statistical analysis

The fluorescence ratio for each array CGH spot was normalized and rescaled into estimated copy number aberrations of each clone according to the comb-fit method (Oba *et al.*, 2006; see also Supplementary Figure S2a). Chromosomal events were detected by locally smoothing variations in copy number aberrations of clones on a chromosome and by applying threshold rules (see Supplementary Figure S2a and Supplementary Information for more detail). The numbers of whole chromosomal events, Nw and of partial chromosomal events, Np, were counted for 22+2 chromosomes in every specimen, and the scatter plot in the Nw–Np plane exhibited apparent three clusters: whole differential dominant ($Nw > Np$), partial differential dominant ($Nw < Np$) and silent ($Nw \approx 0$, $Np \approx 0$) (Supplementary Figure S2b). To discriminate whole differential dominant from partial differential dominant, we defined a 'global' feature variable α as computationally evaluated as the ratio between Nw and Np; when α was small (large), the sample was likely to be whole (partial) differential dominant (see Supplementary Information for more detail). A differential analysis of gene expression was made using standard *t*-test with the *q*-value analysis (Storey and Tibshirani, 2003) for incorporating a false discovery rate (to deal with multiple statistical tests). A survival analysis was made based on Kaplan–Meier and log-rank tests. Univariate and multivariate analyses were made according to the Cox hazard models.

Acknowledgements

We thank institutions and hospitals for providing tumor specimens (see Supplementary Information). We also thank Shigeru Sakiyama, Hiroki Nagase, Iwao Nozawa, Tadayuki Koda and technical staff, past and present, at Division of Biochemistry, Chiba Cancer Center Research Institute. We acknowledge Hisamitsu Pharmaceutical Co. Inc., the Ministry of Education, Culture, Sports, Science and Technology of Japan, the Ministry of Health, Labour and Welfare of Japan and the Hamaguchi Foundation for the Advancement of Biochemistry for funding this work.

References

Albertson DG, Collins C, McCormick F, Gray JW. (2003). Chromosome aberrations in solid tumors. *Nat Genet* **34**: 369 376.

Attiyeh EF, London WB, Mosse YP, Wang Q, Winter C, Khazi D *et al.* (2005). Chromosome 1p and 11q deletions and outcome in neuroblastoma. *N Engl J Med* **353**: 2243 2253.

Bagchi A, Papazoglu C, Wu Y, Capurso D, Brodt M, Francis D *et al.* (2007). CHD5 is a tumor suppressor at human 1p36. *Cell* **128**: 459 475.

Beckwith JB, Perrin EV. (1963). *In situ* neuroblastomas: a contribution to the natural history of neural crest tumors. *Am J Pathol* **43**: 1089 1101.

Brodeur GM. (2003). Neuroblastoma: biological insight into a clinical enigma. *Nat Rev Cancer* **3**: 203 216.

Brodeur GM, Look AT, Shimada H, Hamilton VM, Maris JM, Hann HW *et al.* (2001). Biological aspects of neuroblastomas identified by mass screening in Quebec. *Med Pediatr Oncol* **36**: 157 159.

Brodeur GM, Pritchard J, Berthold F, Carlsen NL, Castel V, Castelberry RP *et al.* (1993). Revisions of the international criteria for neuroblastoma diagnosis, staging, and response to treatment. *J Clin Oncol* **11**: 1466 1477.

Iehara T, Hosoi H, Akazawa K, Matsumoto Y, Yamamoto K, Suita S *et al.* (2006). MYCN gene amplification is a powerful prognostic factor even in infantile neuroblastoma detected by mass screening. *Br J Cancer* **94**: 1510 1515.

Islam A, Kageyama H, Takada N, Kawamoto T, Takayasu H, Isogai E *et al.* (2000). High expression of Survivin, mapped to 17q25, is significantly associated with poor prognostic factors and promotes cell survival in human neuroblastoma. *Oncogene* **19**: 617 623.

Jain AN, Tokuyasu TA, Snijders AM, Segraves R, Albertson DG, Pinkel D. (2002). Fully automatic quantification of microarray image data. *Genome Res* **12**: 325 332.

Kaneko M, Tsuchida Y, Mugishima H, Ohnuma N, Yamamoto K, Kawa K *et al.* (2002). Intensified chemotherapy increases the survival rates in patients with stage 4 neuroblastoma with MYCN amplification. *J Pediatr Hematol Oncol* **24**: 613 621.

Levy IG. (2005). Neuroblastoma, well-designed evaluations, and the optimality of research funding: ask not what your country can do for you. *J Natl Cancer Inst* **97**: 1105 1106.

Look AT, Hayes FA, Nitschke R, McWilliams NB, Green AA. (1984). Cellular DNA content as a predictor of response to chemotherapy in infants with unresectable neuroblastoma. *N Engl J Med* **311**: 231 235.

Maris JM, Matthay KK. (1999). Molecular biology of neuroblastoma. *J Clin Oncol* **17**: 2264 2279.

Nakagawara A. (1998). The NGF story and neuroblastoma. *Med Pediatr Oncol* **31**: 113 115.

Nakagawara A. (2004). Neural crest development and neuroblastoma: the genetic and biological link. *Prog Brain Res* **146**: 233 242.

Nakagawara A, Arima-Nakagawara M, Scavarda NJ, Azar CG, Cantor AB, Brodeur GM. (1993). Association between high levels of expression of the TRK gene and favorable outcome in human neuroblastoma. *N Engl J Med* **328**: 847 854.

Oba S, Tomioka N, Ohira M, Ishii S. (2006). Combfit: a normalization method for array CGH data. *IPSJ Trans Bioinformatics* **47**: 73 82.

Ohira M, Morohashi A, Inuzuka H, Shishikura T, Kawamoto T, Kageyama H *et al.* (2003). Expression profiling and characterization of 4200 genes cloned from primary neuroblastomas: identification of 305 genes differentially expressed between favorable and unfavorable subsets. *Oncogene* **22**: 5525 5536.

Ohira M, Oba S, Nakamura Y, Isogai E, Kaneko S, Nakagawa A *et al.* (2005). Expression profiling using a tumor-specific cDNA microarray predicts the prognosis of intermediate risk neuroblastomas. *Cancer Cell* **7**: 337 350.

Pinkel D, Segraves R, Sudar D, Clark S, Poole I, Kowbel D *et al.* (1998). High resolution analysis of DNA copy number variation using comparative genomic hybridization to microarrays. *Nat Genet* **20**: 207 211.

Sawada T, Hirayama M, Nakata T, Takeda T, Takasugi N, Mori T *et al.* (1984). Mass screening for neuroblastoma in infants in Japan. Interim report of a mass screening study group. *Lancet* **2**: 271 273.

Schwab M, Westermann F, Hero B, Berthold F. (2003). Neuroblastoma: biology and molecular and chromosomal pathology. *Lancet* **4**: 472 480.

Snijders AM, Nowak N, Segraves R, Blackwood S, Brown N, Conroy J *et al.* (2001). Assembly of microarrays for genome-wide measurement of DNA copy number. *Nat Genet* **29**: 263 264.

Srivatsan ES, Ying KL, Seeger RC. (1993). Deletion of chromosome 11 and of 14q sequences in neuroblastoma. *Genes Chromosomes Cancer* **7**: 32 37.

Storey JD, Tibshirani R. (2003). Statistical significance for genome-wide studies. *Proc Natl Acad Sci USA* **100**: 9440 9445.

Tomioka N, Kobayashi H, Kageyama H, Ohira M, Nakamura Y, Sasaki F *et al.* (2003). Chromosomes that show partial loss or gain in near-diploid tumors coincide with chromosomes that show whole loss or gain in near-triploid tumors: evidence suggesting the involvement of the same genes in the tumorigenesis of high- and low-risk neuroblastomas. *Genes Chromosomes Cancer* **36**: 139 150.

Tonini GP. (1993). Neuroblastoma: the result of multistep transformation? *Stem Cells* **11**: 276 282.

Vandesompele J, Van Roy N, Van Gele M, Laureys G, Ambros P, Heimann P *et al.* (1998). Genetic heterogeneity of neuroblastoma studied by comparative genomic hybridization. *Genes Chromosomes Cancer* **23**: 141 152.

Wei JS, Greer BT, Westermann F, Steinberg SM, Son CG, Chen QR *et al.* (2004). Prediction of clinical outcome using gene expression profiling and artificial neural networks for patients with neuroblastoma. *Cancer Res* **64**: 6883 6891.

White PS, Maris JM, Beltinger C, Sulman E, Marshall HN, Fujimori M *et al.* (1995). A region of consistent deletion in neuroblastoma maps within human chromosome 1p36.2 36.3. *Proc Natl Acad Sci USA* **92**: 5520 5524.

Woods WG, Gao RN, Shuster JJ, Robison LL, Bernstein M, Weitzman S *et al.* (2002). Screening of infants and mortality due to neuroblastoma. *N Engl J Med* **346**: 1041 1046.

Supplementary Information accompanies the paper on the Oncogene web site (http://www.nature.com/onc).

Oncogene (2008) 27, 1183–1188

www.nature.com/onc

SHORT COMMUNICATION

ATM-dependent nuclear accumulation of IKK-α plays an important role in the regulation of p73-mediated apoptosis in response to cisplatin

K Yoshida[1,2], T Ozaki[1], K Furuya[1], M Nakanishi[1], H Kikuchi[1], H Yamamoto[1], S Ono[3], T Koda[3], K Omura[2] and A Nakagawara[1]

[1]*Division of Biochemistry, Chiba Cancer Center Research Institute, Chiba, Japan;* [2]*Department of Oral and Maxillofacial Surgery, Tokyo Medical and Dental University, Tokyo, Japan and* [3]*Research Center for Functional Genomics, Hisamitsu Pharmaceutical Co., Inc., Chiba, Japan*

I kappa B kinase (IKK) complex plays an important role in the regulation of signaling pathway that activates nuclear factor–kappa-B (NF-κB). Recently, we reported that cisplatin (CDDP) treatment causes a remarkable nuclear accumulation of IKK-α in association with stabilization and activation of p73. However, underlying mechanisms of CDDP-induced nuclear accumulation of IKK-α are elusive. Here, we found that ataxia–telangiectasia mutated (ATM) is one of upstream mediators of IKK-α during CDDP-induced apoptosis. In response to CDDP, ATM was phosphorylated at Ser-1981, which was accompanied with nuclear accumulation of IKK-α in HepG2 cells, whereas CDDP treatment had undetectable effects on IKK-α in ATM-deficient cells. Indirect immunofluorescence experiments demonstrated that phosphorylated form of ATM colocalizes with nuclear IKK-α in response to CDDP. *In vitro* kinase assay indicated that ATM phosphorylates IKK-α at Ser-473. Moreover, IKK-α-deficient MEFs displayed CDDP-resistant phenotype as compared with wild-type MEFs. Taken together, our present results suggest that ATM-mediated phosphorylation of nuclear IKK-α, which stabilizes p73, is one of the main apoptotic pathways in response to CDDP.
Oncogene (2008) **27**, 1183–1188; doi:10.1038/sj.onc.1210722; published online 13 August 2007

Keywords: apoptosis; ATM; cisplatin; IKK; p73; ubiquitination

I kappa B kinase (IKK) complex, also known as 'signalsome', which includes two highly homologous catalytic subunits (IKK-α and IKK-β) and one regulatory subunit (IKK-γ/NEMO), participates in cytoplasmic signaling pathway that activates prosurvival nuclear factor–kappaB (NF-κB) (Hayden and Ghosh, 2004). A wide variety of extracellular stimuli triggers activation of IKK complex, which phosphorylates IκB and induces its rapid degradation in an ubiquitin/proteasome-dependent manner. NF-κB is then translocated into nucleus, where transcription of its target genes is induced (Karin and Ben-Neriah, 2000). Despite structural similarity between IKK-α and IKK-β, IKK-α knockout mice displayed distinct phenotypes from those of IKK-β-deficient mice (Hu *et al.*, 1999; Li *et al.*, 1999a, b; Takeda *et al.*, 1999). IKK-α-deficient mice exhibited various morphological abnormalities including defective epidermal differentiation; however, cytokine-induced activation of NF-κB was not severely impaired. In contrast, knockout of IKK-β resulted in embryonic lethality, liver degeneration and inhibition of NF-κB activation. In support with these results, IKK-β has an extremely higher activity toward IκB than IKK-α (Huynh *et al.*, 2000). Thus, IKK-β has been considered to be an essential signal transducer in NF-κB activation (Li *et al.*, 1999). Current studies demonstrated that IKK complex undergoes changes in subcellular distribution, suggesting that IKK complex has a novel nuclear function. In contrast to IKK-β, IKK-α accumulated in cell nucleus in response to cytokine exposure and was directly recruited onto the promoter of NF-κB-regulated genes in association with histone H3 phosphorylation (Anest *et al.*, 2003; Yamamoto *et al.*, 2003). Additionally, Verma *et al.* (2004) described that IKK-γ shuttles between cytoplasm and nucleus, and interacts with nuclear co-activator CBP. Wu *et al.* (2006) demonstrated that, upon DNA damage, IKK-γ is phosphorylated by ATM, which encodes a PI3 K family of nuclear Ser/Thr kinase (Kastan and Lim, 2000), and thereby promotes its nuclear export. Recently, we have reported that DNA damage induces nuclear accumulation of IKK-α and nuclear IKK-α stabilizes tumor suppressor p73 (Furuya *et al.*, 2007). However, precise molecular mechanisms behind DNA damage-induced nuclear accumulation of IKK-α have been unclear. In this study, we found that ATM is one of the upstream mediators of nuclear IKK-α in response to DNA damage.

To examine a possible contribution of ATM to DNA damage-induced accumulation of IKK-α, human

Correspondence: Dr A Nakagawara, Division of Biochemistry, Chiba Cancer Center Research Institute, 666-2 Nitona, Chuoh-ku, Chiba 260-8717, Japan.
E-mail: akiranak@chiba-cc.jp
Received 27 April 2007; revised 2 July 2007; accepted 10 July 2007; published online 13 August 2007

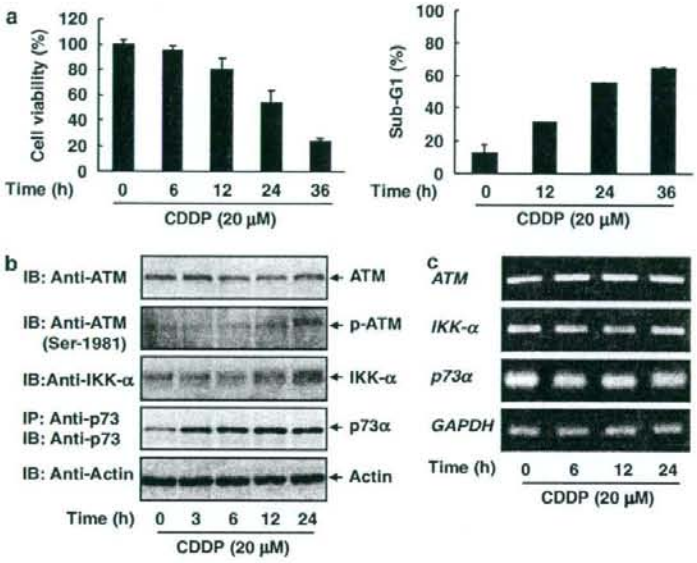

Figure 1 Induction of IKK-α is associated with ATM phosphorylation in response to CDDP. (**a**) CDDP-mediated apoptosis in HepG2 cells. At the indicated time periods after CDDP treatment (20 μM), cell viability and number of cells with sub-G_1 DNA content were examined by MTT (Dojindo) (left panel) and FACS analyses (Becton Dickinson, Oxford, UK) (right panel), respectively. (**b**) Immunoblot analysis. At the indicated time periods after CDDP treatment (20 μM), lysates from HepG2 cells were subjected to immunoblotting (IB) with anti-ATM (Calbiochem, San Diego, CA, USA), anti-phospho-ATM (Cell Signaling, Beverly, MA, USA), anti-IKK-α (Santa Cruz Biotechnology, Santa Cruz, CA, USA) or anti-actin antibody (Sigma, St Louis, MO, USA). Actin expression served as a control for equal protein loading. For p73α, lysates were subjected to immunoprecipitation (IP) with anti-p73 antibody (NeoMarkers, Fremont, CA, USA) followed by IB with anti-p73 antibody. (**c**) RT PCR. At the indicated time points after CDDP treatment (20 μM), total RNA from HepG2 cells was subjected to RT PCR using the indicated primers. *GAPDH* was used as an internal control. PCR products were resolved in 2% agarose gels and visualized by ethidium bromide staining.

hepatocellular carcinoma HepG2 cells were exposed to CDDP. As shown in Figure 1a, HepG2 cells underwent apoptosis in response to CDDP. Immunoblot analysis demonstrated that ATM remains unchanged regardless of CDDP treatment, whereas phospho-ATM increases in response to CDDP (Figure 1b). Consistent with our recent observations (Furuya *et al*., 2007), CDDP treatment resulted in an accumulation of IKK-α as well as p73α, whereas it had undetectable effects on *IKK-α* and p73α mRNAs (Figure 1c). Similar results were also obtained in p53-deficient human lung carcinoma H1299 cells (Supplementary Figure S1). As described (Saito *et al*., 2002; Kurz *et al*., 2004), CDDP-induced phosphorylation of ATM and p53 was significantly blocked by wortmannin (Figure 2a). Of note, wortmannin treatment led to a remarkable inhibition of CDDP-dependent accumulation of IKK-α and p73α. Expectedly, CDDP-induced nuclear accumulation of IKK-α was strongly blocked in cells exposed to wortmannin (Figure 2b), suggesting that ATM might act as one of the upstream mediators of IKK-α in response to DNA damage. In support with this notion, CDDP treatment had negligible effects on IKK-α and p73α in ATM-deficient A-T cells (Figure 2c). *IKK-α* and p73α mRNAs remained unchanged in A-T cells treated with CDDP (Figure 2d). Additionally, enforced expression of ATM resulted in an induction of nuclear IKK-α (Supplementary Figure S2).

Since cytoplasmic IKK-α remained constant in HepG2 cells exposed to CDDP, CDDP-induced nuclear translocation of IKK-α might not occur. To address whether IKK-α could be regulated in a proteasome-dependent manner, human osteosarcoma U2OS cells were treated with proteasome inhibitor MG-132 and then analysed for IKK-α. Immunoblot of p53 was performed as a positive control. As shown in Figure 3a, MG-132 treatment caused a significant accumulation of IKK-α. Similar results were also obtained in U2OS cells treated with lactacystin (data not shown). Next, U2OS cells were exposed to MG-132 and fractionated into nuclear and cytoplasmic fractions followed by immunoblotting. As seen in Figure 3b, nuclear and cytoplasmic IKK-α were stabilized by MG-132. To examine whether IKK-α could be regulated by ubiquitin/proteasome system, U2OS cells were co-transfected with IKK-α expression plasmid together with His-tagged ubiquitin. Twenty-four hours after transfection, cells were treated with CDDP for 24 h or left untreated followed by an

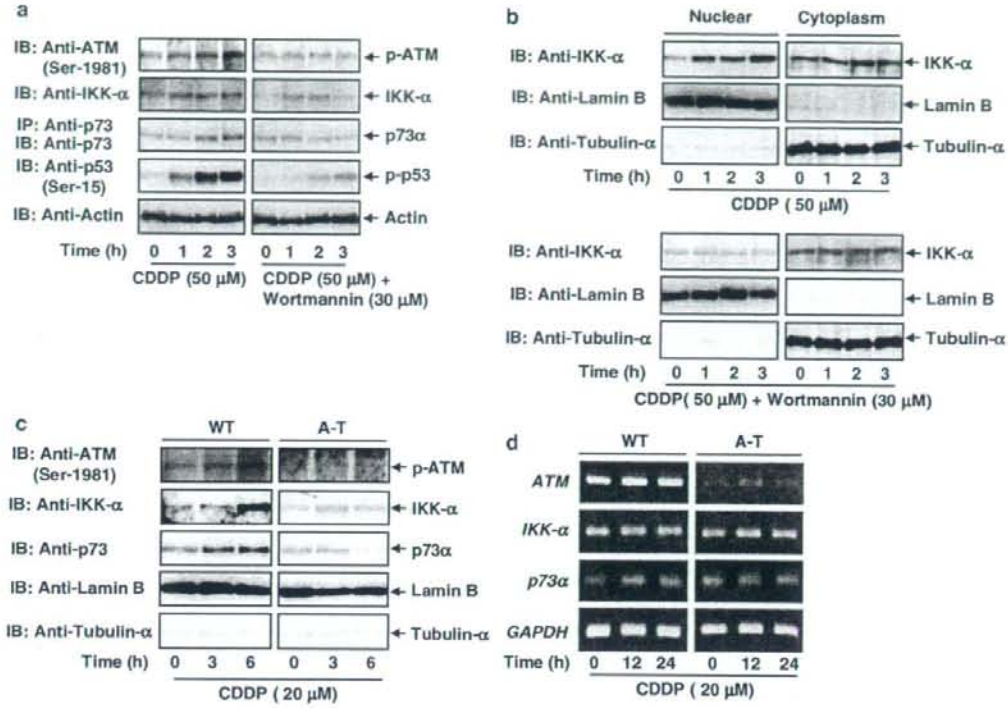

Figure 2 ATM is required for CDDP-mediated induction of IKK-α and p73. (**a**) Wortmannin inhibits accumulation of IKK-α and p73 in response to CDDP. At the indicated time periods after CDDP treatment (50 μM) together with (right panels) or without 30 μM of wortmannin (Sigma) (left panels), lysates from HepG2 cells were processed for IB with anti-phospho-ATM, anti-IKK-α, anti-phospho-p53 (Cell Signaling) or anti-actin antibody. For p73α, lysates were IP with anti-p73 antibody followed by IB with anti-p73 antibody. (**b**) CDDP-mediated nuclear accumulation of IKK-α is inhibited by wortmannin. HepG2 cells were exposed to 50 μM of CDDP in the absence (upper panels) or presence (lower panels) of 30 μM of wortmannin. At the indicated time periods after treatment, cells were fractionated into nuclear and cytoplasmic fractions and then analysed for IKK-α by IB. Anti-Lamin B (Oncogene Research Products) and anti-tubulin-α (NeoMarkers) IB were performed to assess purify of each fraction. (**c**) Immunoblot analysis. Wild-type or ATM-deficient A-T cells were exposed to 20 μM of CDDP. At the indicated time points after CDDP treatment, nuclear extracts were subjected to IB with the indicated antibodies. (**d**) RT PCR. At the indicated time periods after CDDP treatment (20 μM), total RNA was subjected to RT PCR for ATM, IKK-α and p73α.

exposure to MG-132 for 6 h, and ubiquitinated materials were recovered by nickel agarose and then analysed by immunoblotting. As shown in Figure 3c, ubiquitinated forms of IKK-α were detectable under normal conditions, whereas they were significantly reduced in cells exposed to CDDP. Taken together, our results suggest that CDDP treatment stabilizes nuclear IKK-α by blocking ubiquitin/proteasome-dependent degradation system.

To investigate whether there could exist a functional interaction between IKK-α and ATM, we examined their subcellular localization. U2OS cells were transfected with FLAG-IKK-α expression plasmid. Thirty-six hours after the transfection, cells were treated with CDDP for 12 h or left untreated and simultaneously stained with anti-phospho-ATM and anti-FLAG antibodies. As shown in Figure 4a, phospho-ATM became detectable in nucleus in response to CDDP. FLAG-IKK-α was largely expressed in cytoplasm without CDDP, whereas CDDP treatment led to an accumulation of FLAG-IKK-α in nucleus. Merged images indicated nuclear colocalization of phospho-ATM and FLAG-IKK-α. Immunoprecipitation experiments indicated that the endogenous ATM forms a complex with IKK-α in cells (Supplementary Figure S3). Next, we investigated whether ATM could phosphorylate IKK-α. As described (Kastan and Lim, 2000), ATM phosphorylates Ser/Thr followed by Glu. According to our extensive search of the amino acid residues of IKK-α, we found six putative ATM-dependent phosphorylation sites (Figure 4b). *In vitro* kinase assay using anti-ATM immunoprecipitates from HeLa cells exposed to CDDP revealed that GST-IKK-α (335–745) but not GST-IKK-α (2–334) is phosphorylated by anti-ATM

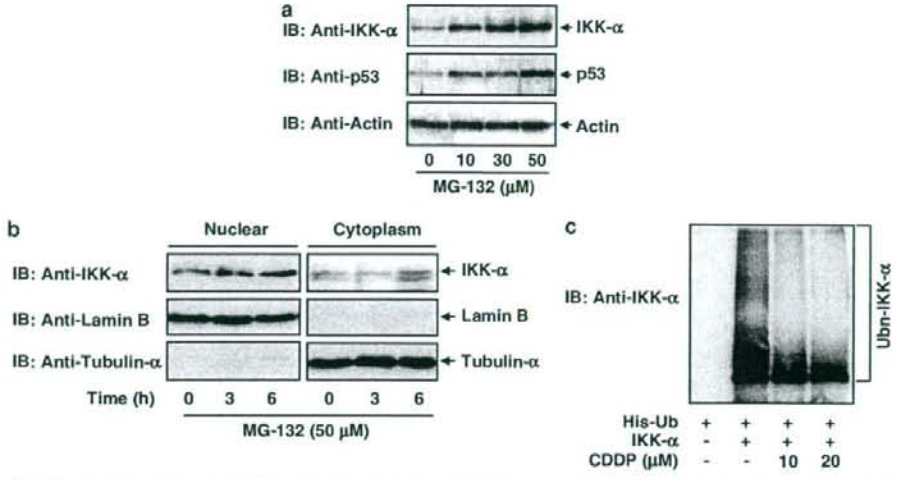

Figure 3 CDDP treatment impairs ubiquitination of IKK-α. (**a**) IKK-α is stabilized by proteasome inhibitor. U2OS cells were exposed to the indicated concentrations of MG-132 (Calbiochem). Six hours after treatment, lysates were processed for IB with the indicated antibodies. (**b**) Nuclear IKK-α is regulated in a proteasome-dependent manner. U2OS cells were treated with 50 μM of MG-132 for 6 h and then fractionated into nuclear and cytoplasmic fractions followed by IB with the indicated antibodies. (**c**) CDDP-induced reduction in ubiquitination levels of IKK-α. Expression plasmid for IKK-α was introduced into U2OS cells along with His-ubiquitin (His-Ub) and treated with or without CDDP at the indicated concentrations. Ubiquitinated materials were recovered by nickel agarose (Qiagen, Valencia, CA, USA) and separated by SDS PAGE followed by IB with anti-IKK-α antibody.

immunoprecipitates (data not shown). Thus, we focused on GST-IKK-α (335–745) and generated the indicated GST-IKK-α (335–745) mutants where Ser was substituted to Ala (Figure 4c). Unfortunately, *Escherichia coli* did not express IKK-α (T659A). Each of these GST fusion proteins except IKK-α (T659A) was incubated with anti-ATM immunoprecipitates prepared from CDDP-treated HeLa cells in the presence of [γ-^{32}P]ATP. Reaction mixtures were then separated by sodium dodecyl sulphate–polyacrylamide gel electrophoresis followed by autoradiography. As shown in Figure 4c, anti-ATM immunoprecipitates phosphorylated IKK-α (S351A), IKK-α (S369A) and IKK-α (S596A). In contrast, IKK-α (S473A) was labeled to a lesser degree. Collectively, our results suggest that ATM phosphorylates IKK-α at Ser-473 in response to CDDP.

We then asked whether IKK-α could affect CDDP sensitivity. At the indicated time points after CDDP treatment, cell viability of wild-type MEFs and MEFs from IKK-α knockout mice (Begg *et al.*, 1995) was examined by MTT assay. As shown in left panel of Figure 4d, IKK-α-deficient MEFs displayed CDDP-resistant phenotype relative to wild-type MEFs, suggesting that IKK-α plays a critical role in the regulation of DNA damage response. Immunoblot analysis demonstrated that CDDP-mediated phosphorylation of ATM is detectable in both MEFs (right panel of Figure 4d). Consistent with our recent observations (Furuya *et al.*, 2007), CDDP-mediated accumulation of IKK-α and p73α was detectable in wild-type MEFs. In contrast, p73α remained constant in IKK-α-deficient MEFs exposed to CDDP. Thus, it is likely that ATM transmits apoptotic signal through nuclear IKK-α, and thereby promotes the stabilization of pro-apoptotic p73.

Our results indicated that Ser-473 of IKK-α is at least one of the potential targets of ATM-mediated phosphorylation in response to CDDP. Accumulating evidence suggests that the activation of IKK complex is dependent on its phosphorylation (Hayden and Ghosh, 2004). Delhase *et al.* (1999) described that IKK-β is autophosphorylated at its C-terminal region to regulate its activity. Alternatively, NF-κB-inducing kinase (NIK) directly phosphorylates and activates IKK-α (Regnier *et al.*, 1997). Intriguingly, Li *et al.* (2001) reported that ATM is required for DNA damage-induced activation of IKK-α, which supports our present results. Another finding of our present study is that CDDP-mediated nuclear accumulation of IKK-α is regulated in an ubiquitin/proteasome-dependent manner. In response to DNA damage, p53 is phosphorylated at its N-terminal region, which blocks MDM2-mediated ubiquitination of p53 (Vousden and Lu, 2002), raising a possibility that ATM-mediated phosphorylation of IKK-α might inhibit its ubiquitination and subsequent degradation through ubiquitin/proteasome pathway. Further work should be necessary to resolve this issue.

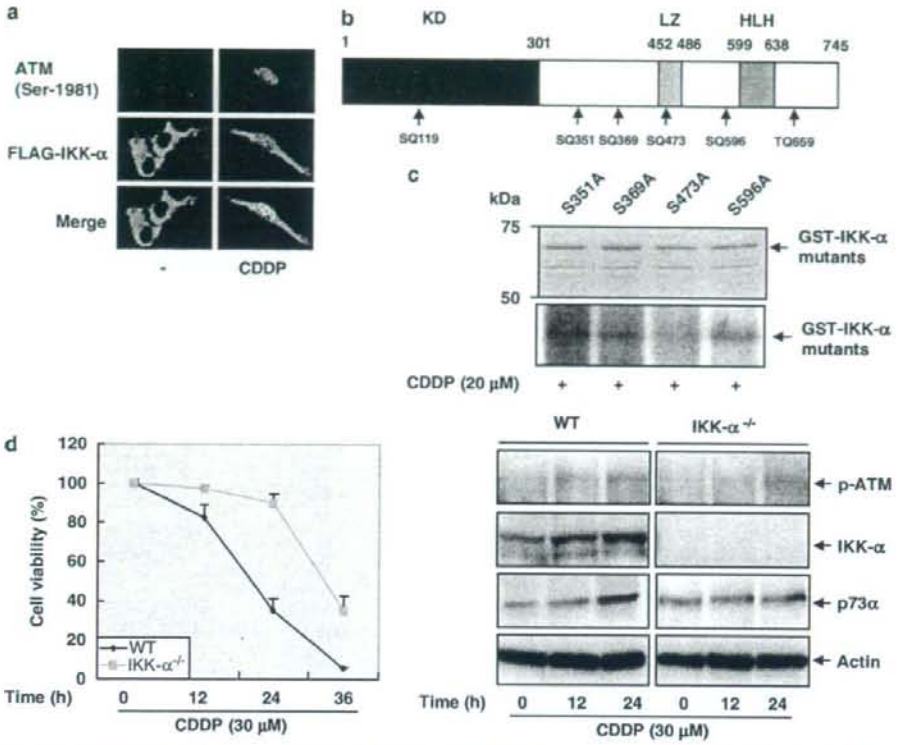

Figure 4 ATM-mediated phosphorylation of IKK-α. (**a**) U2OS cells were transfected with expression plasmid for FLAG-IKK-α using LipofectAMINE 2000 (Invitrogen, Carlsbad, CA, USA). Thirty-six hours after transfection, cells were treated with 20 μM of CDDP for 12 h or left untreated and then processed for indirect immunostaining with anti-phospho-ATM and anti-FLAG antibodies (Sigma). Merged images indicate nuclear colocalization of phospho-ATM and FLAG-IKK-α. (b) Domain structure of IKK-α. KD, kinase domain; LZ, leucine-zipper domain; HLH, helix loop helix domain. Numbers indicate amino acid position. Putative ATM-dependent phosphorylation sites of IKK-α are also indicated. (**c**) *In vitro* kinase assay. cDNA fragments encoding IKK-α (335 745) bearing the indicated mutations were amplified by PCR (Invitrogen) and then inserted into *Eco*RI/*Xho*I sites of pGEX plasmid (Amersham Biosciences, Uppsala, Sweden) to give IKK-α (S351A), IKK-α (S369A), IKK-α (S473A) and IKK-α (S596A). Upper panel shows expressions of the indicated GST fusion proteins. For *in vitro* kinase reaction, lysates from HeLa cells exposed to CDDP (20 μM) for 24 h were IP with anti-ATM antibody and anti-ATM immunoprecipitates were incubated with the indicated GST fusion proteins in the presence of [γ-^{32}P]ATP (Amersham Biosciences) at 30°C for 30 min. Reaction mixtures were then processed for SDS PAGE. After electrophoresis, the gel was dried and exposed to an X-ray film at room temperature (lower panel). (**d**) IKK-α contributes to CDDP sensitivity. Wild-type and IKK-α-deficient MEFs were exposed to 30 μM of CDDP. At the indicated time periods after CDDP treatment, cell viability was examined by MTT assay (left panel). For IB, lysates from the indicated MEFs treated with 30 μM of CDDP for the indicated time periods were subjected to IB with anti-phospho-ATM, anti-IKK-α or anti-actin antibody. For p73α, the indicated lysates were IP with anti-p73 followed by IB with anti-p73 antibody (right panel).

Acknowledgements

This work was supported in part by a Grant-in-Aid from the Ministry of Health, Labour and Welfare for the Third Term Comprehensive Control Research for Cancer, a Grant-in-Aid for Scientific Research on Priority Areas from the Ministry of Education, Culture, Sports, Science and Technology, Japan, a Grant-in-Aid for Scientific Research from Japan Society for the Promotion of Science and Uehara Memorial Foundation.

References

Anest V, Hanson JL, Cogswell PC, Steinbrecher KA, Strahl BD, Baldwin AS. (2003). A nucleosomal function for IkappaB kinase-alpha in NF-kappaB-dependent gene expression. *Nature* **423**: 659 663.

Begg AA, Sha WC, Bronson RT, Ghosh S, Baltimore D. (1995). Embryonic lethality and liver degeneration in mice lacking the RelA component of NF-kappa B. *Nature* **376**: 167 170.

Delhase M, Hayakawa M, Chen Y, Karin M. (1999). Positive and negative regulation of IkappaB kinase activity through IKKbeta subunit phosphorylation. *Science* **284**: 309 313.

Furuya K, Ozaki T, Hanamoto T, Hosoda M, Hayashi S, Barker PA *et al*. (2007). Stabilization of p73 by nuclear IKK-α mediates cisplatin-induced apoptosis. *J Biol Chem* **282**: 18365 18378.

Hayden MS, Ghosh S. (2004). Signaling of NF-kappaB. *Genes Dev* **18**: 2149 2224.

Hu Y, Baud V, Delhase M, Zhang P, Deerinck T, Ellisman M *et al.* (1999). Abnormal morphogenesis but intact IKK activation in mice lacking the IKKα subunit of IκB kinase. *Science* **284**: 316 320.

Huynh QK, Boddupalli H, Rouw SA, Koboldt CM, Hall T, Sommers C *et al.* (2000). Characterization of the recombinant IKK1/IKK2 heterodimer. Mechanisms regulating kinase activity. *J Biol Chem* **275**: 25883 25891.

Karin M, Ben-Neriah Y. (2000). Phosphorylation meets ubiquitination: the control of NF-κB activity. *Annu Rev Immunol* **18**: 621 663.

Kastan MB, Lim D. (2000). The many substrates and functions of ATM. *Nat Rev Mol Cell Biol* **1**: 179 186.

Kurz EU, Douglas P, Lees-Miller SP. (2004). Doxorubicin activates ATM-dependent phosphorylation of multiple downstream targets in part through the generation of reactive oxygen species. *J Biol Chem* **279**: 53272 53281.

Li N, Banin S, Ouyang H, Li GC, Courtois G, Shiloh Y *et al.* (2001). ATM is required for IκB kinase (IKK) activation in response to DNA double strand breaks. *J Biol Chem* **276**: 8898 8903.

Li Q, Lu O, Hwang JY, Busher D, Lee KF, Izpisua-Belmonte JC *et al.* (1999a). IKK1-deficient mice exhibit abnormal development of skin and skeleton. *Genes Dev* **13**: 1322 1328.

Li Q, Van Antwerp D, Mercurio F, Lee KF, Verma IM. (1999b). Severe liver degeneration in mice lacking the IkappaB kinase 2 gene. *Science* **284**: 321 325.

Regnier CH, Song HY, Gao X, Goeddel DV, Cao Z, Rothe M. (1997). Identification and characterization of an IκB kinase. *Cell* **90**: 373 383.

Saito S, Goodarzi AA, Higashimoto Y, Noda Y, Lees-Miller SP, Appella E *et al.* (2002). ATM mediates phosphorylation at multiple p53 sites, including Ser(46), in response to ionizing radiation. *J Biol Chem* **277**: 12491 12494.

Takeda K, Takeuchi O, Tsujimura T, Itami S, Adachi O, Kawai T *et al.* (1999). Limb and skin abnormalities in mice lacking IKKα. *Science* **284**: 313 316.

Tanaka M, Fuentes ME, Yamaguchi K, Durnin MH, Dalrymple SA, Hardy KL *et al.* (1999). Embryonic lethality, liver degeneration, and impaired NF-kappa B activation in IKK-beta-deficient mice. *Immunity* **10**: 421 429.

Verma UN, Yamamoto Y, Prajapati S, Gaynor RB. (2004). Nuclear role of I kappa B kinase-gamma/NF-kappa B essential modulator (IKK gamma/NEMO) in NF-kappa B-dependent gene expression. *J Biol Chem* **279**: 3509 3515.

Vousden KH, Lu X. (2002). Live or let die: the cell's response to p53. *Nat Rev Cancer* **2**: 594 604.

Wu ZH, Shi Y, Tibbetts RS, Miyamoto S. (2006). Molecular linkage between the kinase ATM and NF-kappaB signaling in response to genotoxic stimuli. *Science* **311**: 1141 1146.

Yamamoto Y, Verma UN, Prajapati S, Kwak YT, Gaynor RB. (2003). Histone H3 phosphorylation by IKK-alpha is critical for cytokine-induced gene expression. *Nature* **423**: 655 659.

Supplementary Information accompanies the paper on the Oncogene website (http://www.nature.com/onc).

Oncogene (2008) 27, 741–754

www.nature.com/onc

ORIGINAL ARTICLE

Stress via p53 pathway causes apoptosis by mitochondrial Noxa upregulation in doxorubicin-treated neuroblastoma cells

K Kurata[1], R Yanagisawa[1], M Ohira[2], M Kitagawa[3], A Nakagawara[2] and T Kamijo[1,2]

[1]Department of Pediatrics, Shinshu University School of Medicine, Matsumoto, Nagano, Japan; [2]Division of Biochemistry, Chiba Cancer Center Research Institute, Chuoh-ku, Chiba, Japan and [3]Department of Biochemistry, Hamamatsu University School of Medicine, Hamamatsu, Shizuoka, Japan

In this study, we employed a panel of cell lines to determine whether p53-dependent cell death in neuroblastoma (NB) cells is caused by apoptotic cellular function, and we further studied the molecular mechanism of apoptosis induced via the p53-dependent pathway. We obtained evidence that a type of p53-dependent stress, doxorubicin (Doxo) administration, causes accumulation of p53 in the nucleus of NB cells and phosphorylation of several serine residues in both Doxo-sensitive and -resistant cell lines. Upregulation of p53-downstream molecules in cells and upregulation of Noxa in the mitochondrial fraction were observed only in Doxo-sensitive NB cells. Significance of Noxa in the Doxo-induced NB cell death was confirmed by Noxa-knockdown experiments. Mitochondrial dysfunction, including cytochrome-*c* release and membrane potential disregulation, occurred and resulted in the activation of the intrinsic caspase pathway. However, in the Doxo-resistant cells, the accumulation in the nucleus and phosphorylation of p53 did not induce p53-downstream $p21^{Cip1/Waf1}$ expression and the Noxa upregulation, resulting in the retention of the mitochondrial homeostasis. Taken together, these findings indicate that the p53 pathway seems to play a crucial role in NB cell death by Noxa regulation in mitochondria, and inhibition of the induction of p53-downstream effectors may regulate drug resistance of NB cells.
Oncogene (2008) **27**, 741–754; doi:10.1038/sj.onc.1210672; published online 20 August 2007

Keywords: neuroblastoma; p53; noxa; mitochondria; apoptosis

Introduction

Neuroblastoma (NB) is the most common pediatric solid malignant tumor derived from the sympathetic nervous system. Unlike the many childhood malignancies for which survival has been improved by recent therapies, high-risk NB is still one of the most difficult tumors to cure, with only 30% long-term survival despite intensive multimodal therapy. New treatments and a better understanding of drug resistance mechanisms are required for the improvement of the survival rate. A noteworthy finding of NB research is that mutations of p53 tumor suppressor have been reported in less than 2% of NBs out of 340 tested (Tweddle *et al.*, 2001). Instead of mutation, cytoplasmic sequestration of p53 has been proposed as an alternative mechanism of inactivation in NB cells. The sequestration was first detected in frozen tumor samples using immunohistochemical techniques (Moll *et al.*, 1995) and later in NB cell lines by immunofluorescence and cell fractionation experiments (Moll *et al.*, 1996). However, several groups reported nuclear p53 accumulation in NB cells harboring wild-type p53 after DNA damage (Tweddle *et al.*, 2003). After nuclear accumulation, p53 phosphorylation, binding to targeted sequences and transcriptional transactivation are sequentially induced by DNA damage in *p53* wild-type cells (Oren, 1999). However, these processes in NB cells harboring wild-type p53 have not been examined with respect to the role of p53 pathways in the tumorigenesis of NB. Their examination should also yield insights into the molecular mechanisms of p53 inactivation. For instance, upregulation of the p53-downstream genes encoding $p21^{Cip1/Waf1}$ and HDM2 in *p53* wild-type NB cell lines was observed in several studies (Isaacs *et al.*, 2001; Keshelava *et al.*, 2001; Tweddle *et al.*, 2001) but not all (Wolff *et al.*, 2001). Reporter gene assays detected p53 transcriptional function in one study (Keshelava *et al.*, 2001) but not in another (Wolff *et al.*, 2001). Together, these facts indicate that systematic and detailed analysis of the biological effects of p53-dependent stress on the cell death of NB cells and of the mechanisms of activation and signal transduction of p53-related pathways in NB cells are required for understanding the mechanism of drug resistance and for the development of new therapies for high-risk NB patients.

The Bcl-2 family member proteins regulate mitochondrial cell death by controlling mitochondrial outer membrane permeabilization (MOMP). Anti-apoptotic Bcl-2 family members (for example, Bcl-2, Bcl-xL, Bcl-w and Mcl-1) function to block MOMP, whereas the

Correspondence: Dr T Kamijo, Division of Biochemistry, Chiba Cancer Center Research Institute, 666-2 Nitona, Chuoh-ku, Chiba 260-8717, Japan.
E-mail: tkamijo@chiba-cc.jp
Received 4 December 2006; revised 1 June 2007; accepted 11 June 2007; published online 20 August 2007

various pro-apoptotic proteins promote it. The pro-apoptotic proteins fall into two general subfamilies, based on the sharing of Bcl-2 homology domains. BH123 proteins appear to be effectors of MOMP, because cells from mice lacking the two major BH123 proteins, Bax and Bak, fail to undergo MOMP in response to a wide range of apoptotic stresses (Wei *et al*., 2001). The other subfamily, the BH3-only proteins, can act either to activate Bax or Bak or to interfere with the anti-apoptotic Bcl-2 family members (Letai *et al*., 2002). Noxa is a BH3-only member of Bcl-2 family proteins (Oda *et al*., 2003) and its expression is induced by DNA damage such as that caused by etoposide or doxorubicin in a p53-dependent manner (Oda *et al*., 2003; Shibue *et al*., 2003). Furthermore, several lines of evidence reported that Noxa is one of the most important cell death effectors in neuronal cell death, for example, nuclear factor-kappa B modulated cell death in mouse cortical neurons (Aleyasin *et al*., 2004), axotomized motor neurons of adult mouse (Kiryu-Seo *et al*., 2005), sensory neurons especially in trigeminal ganglia and cervical dorsal ganglia (Hudson *et al*., 2005) and arsenite-induced cortical neurons (Wong *et al*., 2005).

These results have led us to study the role and molecular machinery of p53-dependent cell death in NB by utilizing several *p53* wild-type NB cell lines. We studied the sensitivities of NB cell lines to doxorubicin (Doxo), which is a representative cytotoxic drug against NB cells (Matthay *et al*., 1998) that induces stresses that are basically dependent on p53 (Lowe *et al*., 1994), and transactivates p53 and its downstream effectors in many tissues (Komarova *et al*., 1997). In sensitive NB cells, the following important findings were observed after Doxo treatment: (1) accumulation of p53 in the nucleus; (2) activation of the p53-downstream molecules; (3) pro-apoptotic BH3-only Bcl-2 family protein Noxa induction and upregulation in mitochondria resulting in mitochondrial dysfunction/intrinsic caspase-derived apoptosis. Although p53 accumulated in the nucleus before Doxo treatment, the downstream molecules were not induced and the upregulation of Noxa in mitochondria was not observed in the Doxo-resistant NB cells. Consequently, the crucial role of the p53 pathway in apoptosis in NB cells was indicated by our observations.

Results

Heterogeneity of response to p53-dependent death signals in NB cell lines harboring wild-type p53

We chose 0.5 μg/ml of Doxo as an appropriate concentration to assess the effect of Doxo on NB cells according to the results of the analysis of peak plasma concentrations of doxorubicin (Hempel *et al*., 2002). Similar results were obtained by 0.3–1.0 μg/ml of Doxo in the following experiments (data not shown). Trypan blue uptake assays were performed to compare the Doxo sensitivity of NB cell lines harboring wild-type *p53* (Figure 1a). More than 60% of cells were Trypan blue-positive for the SH-SY5Y, NB9, NB69 and SK-N-SH NB cell lines 36 h after Doxo stimulation. On the other hand, less than 40% of cells were positive in NB-19 and NB1 cell lines and less than 10% in IMR32 cells even 36 h after Doxo stimulation.

Next, we performed WST-8 assay, a modification of MTT assay, to evaluate cytotoxicity on NB cells (Figure 1b). We confirmed the sensitivity of NB cells to Doxo by these experiments and also studied the effects of etoposide, the other p53-dependent damage-inducing reagent, on NB cells. Etoposide was effectively cytotoxic on the Doxo-sensitive SK-N-SH, SH-SY5Y, NB-9 and NB-69 cells. In the Doxo-resistant NB cells, IMR32 and NB-1 cells also possessed drug resistance against etoposide, whereas NB-19 cells had sensitivity.

FACS analysis of sub-G_0/G_1 cells showed that considerable percentages of cells underwent apoptosis 24 h after the Doxo treatment in SH-SY5Y, NB-9, NB-69 and SK-N-SH (Figure 1c). However, the proportions of apoptotic cells were significantly lower in NB-19, NB-1 and IMR32 than in the four Doxo-sensitive NB cell lines. In SK-N-SH and SH-SY5Y cells, the increase of the sub-G_0/G_1 fraction after Doxo treatment was confirmed by the condensation and fragmentation of nuclei (Figure 1d). In contrast, almost all of the nuclei were intact in the resistant IMR32 and NB-1 cells. Thus, Doxo-induced stresses resulted in apoptosis in some NB cells, whereas others were resistant (Figure 1).

Upregulation and nuclear accumulation of p53 are not enough to induce apoptosis by Doxo treatment

To study the basis of the different sensitivities of NB cells to p53-dependent stress, we first performed direct western blot analysis using a monoclonal antibody recognizing the p53 N terminus (DO1) to estimate the total amount of p53. We also used antibodies that specifically react with phosphorylated serine residues (Ser15, Ser20 and Ser46) to examine the modulation of the stability and/or activity of p53 in response to DNA damage.

The amount of p53 was clearly increased by Doxo in the Doxo-sensitive NB cells, as detected with DO1 antibody (Figure 2a). p53 accumulation was observed in the Doxo-resistant IMR32 and NB-19 cells before treatment; serine15 phosphorylation was induced in all the NB cells after Doxo exposure. Upregulation of serine46 phosphorylation was also observed in the NB cell lines, except for IMR32 and SH-SY5Y cells. On the other hand, ser20 phosphorylation was not strongly upregulated in any of the lines. Consistent with previous reports, RT–PCR analysis showed that the induction of p53 protein by Doxo treatment in sensitive-NB cells was not caused at the transcriptional level (Figure 2b). Thus, it appears that the upregulation of p53 protein in Doxo-treated NB cells seemed to be caused by protein stabilization.

Next, we investigated the localization of p53 in NB cells, using DO1 as a human p53-specific antibody reacting with amino acids 21–25, pAb421 as a pan-p53 antibody reacting with the human p53 amino acids 370–378 and

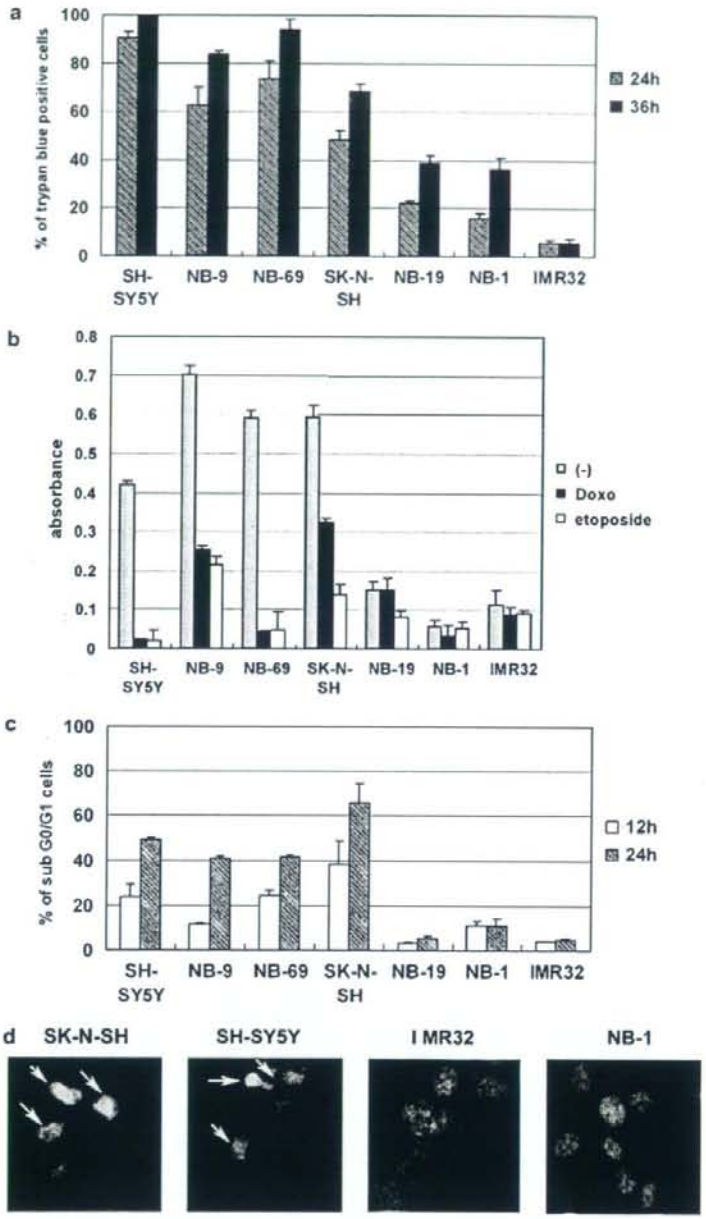

Figure 1 Sensitivity to doxorubicin (Doxo) is heterogenic in wild-type p53 harboring neuroblastoma (NB) cells. One hundred thousand cells were plated in a 3-cm-diameter culture dish and cultured in 5% CO_2 for 24 h. Doxo was added to the dish at 0.5 μg/ml and the incubation was continued for the indicated times. Mean and standard deviation (s.d.) of the % of cells were calculated for triplicate samples. (**a**) Cells were washed with 1 × phosphate-buffered saline (PBS), collected by 1 × PBS/0.5 mM EDTA, and stained with Trypan blue. The results are representative of four independent experiments. (**b**) After treatment of DNA-damaging reagents, cell viabilities were analysed by WST-8 assay. The results are representative of at least three independent experiments. (**c**) Analysis of the sub-G_0/G_1 fraction was performed as described in Materials and methods. The results are representative of three independent experiments. (**d**) Staining with 4′,6-diamidino-2-phenylindole (DAPI) was performed 24 h after Doxo stimulation. Arrows indicate the condensed or fragmented nuclei.

16G8 as an anti-phosphorylated p53ser15 antibody. Staining with pAb421 antibody revealed that the punctate cytoplasmic signal was upregulated in both Doxo-sensitive and -resistant NB cells after Doxo exposure (Figure 2c). DO1 antibody showed both nuclear and cytoplasmic staining before treatment, and remarkable accumulation into the nucleus was induced by Doxo in these four NB cell lines. Although ser15 phosphorylation was hardly

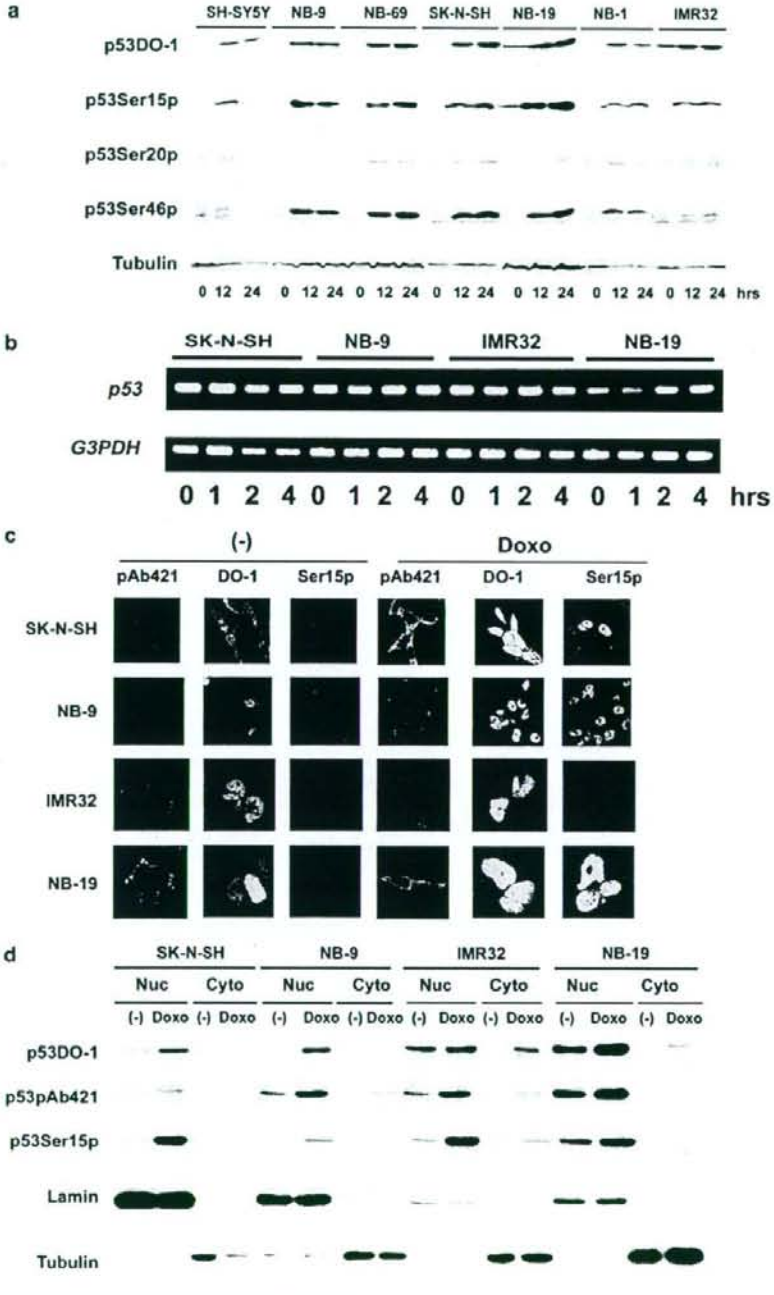

detected before treatment, the phosphorylation was remarkably upregulated by Doxo in SK-N-SH, NB-9 and NB-19 cells. In IMR32 cells, p53ser15 phosphorylation was modestly upregulated. The ser15-phosphorylated p53 accumulated to a much greater degree in the nucleus than in the cytoplasm after Doxo treatment. The use of several different fixation methods and modification of the first antibody concentration did not influence the results of immunofluorescence. Moreover, *p53* wild-type MCF7 cells showed similar staining results with these antibodies (data not shown). To investigate the observed discrepancy of p53 localization among the three monoclonal antibodies in the immunofluorescence experiments, we performed cell fractionation experiments (Figure 2d). All of the p53 signals were detected only in the nucleus before the treatment, and the upregulated signals induced by Doxo also accumulated in the nucleus rather than in the cytoplasm. The controls for fractionation, the nuclear marker lamin and cytoplasmic marker β-tubulin, were detected in the proper fractions and the amounts were not changed by Doxo treatment. These results show that the p53-dependent Doxo-stress increased the amount of p53 and induced the accumulation of p53 in the nucleus in both Doxo-sensitive and -resistant NB cells.

Activity of p53 as a transcriptional factor is required for Doxo-induced NB apoptosis

We then assessed the induction of p53-downstream molecules by Doxo. As shown in Figure 3a, exposure to Doxo induced remarkable $p21^{Cip1/Waf1}$ protein accumulation in the sensitive cells but not in the resistant cells, and this induction was caused at the transcriptional level (Figure 3b). HDM2 was similarly induced by Doxo treatment in the sensitive cells. However, *HDM2* mRNA accumulated in the resistant cells before Doxo treatment and did not change subsequently (Figure 3b), which is consistent with its protein accumulation (Figure 3a). These results indicate that the Doxo-induced cellular stress can effectively induce the p53 transcriptional activities in Doxo-sensitive NB cells but not in the resistant cells.

Doxo treatment induces synthesis of pro-apoptotic Noxa in the sensitive NB cells but not in the resistant cells

Next, we studied the expression of Bcl-2 family proteins in the NB cells, because regulation of the Bcl-2 family proteins by p53 is known to be the main component of p53-dependent apoptosis (Shen and White, 2001). The pro-apoptotic Bcl-2 family proteins Bax, Bak and Bok were not modified by Doxo in the NB cells (Figure 3a). Expression of Puma and p53AIP1 was also not affected by Doxo treatment (data not shown). It is interesting that Noxa was substantially induced only in the sensitive cells but not in the resistant cells. Although there was a considerable difference in the amount of anti-apoptotic Bcl-2 among the NB cells, its expression seemed not to be related to the Doxo sensitivity. The other anti-apoptotic Bcl-2 family protein Bcl-xL was not detected in any of the NB cells (data not shown). To assess whether the induction of Noxa is regulated at the transcriptional level, we performed semi-quantitative RT–PCR analysis. Consistent with the results of the western blot analysis, the mRNA amount of Noxa was clearly upregulated by Doxo treatment in the Doxo-sensitive SK-N-SH cells (Figure 3b). Meanwhile, the accumulation of *Noxa* mRNA expression was detected in the resistant cells (Figure 3b) and confirmed by quantitative real-time PCR analysis (Figure 3c). However, *Noxa* mRNA was not increased by Doxo treatment in the resistant cells (Figure 3b).

Noxa accumulation in mitochondria is not sufficient to induce apoptosis in NB cells

A recent report demonstrated that Noxa and Bok were induced by DNA stress dependent upon the p53 pathway in the SH-SY5Y cell line (Yakovlev *et al*., 2004). However, only Noxa upregulation was detected in the present study in the sensitive NB cell lines. Interestingly, larger amounts of Noxa were observed in the Doxo-resistant NB lines (IMR32 and NB-19) compared with the sensitive lines (SK-N-SH and NB-9). Since the organelle-specific amounts of the pro-apoptotic Bcl-2 family protein and its ratio to anti-apoptotic Bcl-2 family proteins in mitochondria are reported to determine cell fate in mitochondria-dependent apoptosis (Nakazawa *et al*., 2003; Danial and Korsmeyer, 2004), we studied the amounts of Noxa in mitochondria by cell fractionation/western blot analysis (Figure 4A). The amounts of Noxa in mitochondria were apparently upregulated in the sensitive cells. Densitometric analysis revealed that the Doxo-treatment increased the content of Noxa 10.3-fold in SK-N-SH cells and 16.6-fold in NB-9 cells compared to that before stimulation. On the other hand, Noxa was accumulated at higher levels in mitochondria of the resistant cells compared with the sensitive cells before Doxo treatment, and was not further increased by Doxo treatment. There were no significant differences in the amounts of Bcl-2 in the presence or absence of Doxo

Figure 2 Upregulation and nuclear accumulation of p53 in neuroblastoma (NB) cells. (**a**) Cells were collected after Doxo stimulation at the indicated time points (0, 12 and 24 h) and analysed by western blotting with the indicated antibodies (DO-1, p53ser15p, p53ser20p, p53ser46p and β-tubulin) as described in Materials and methods. (**b**) Cells were collected after Doxo stimulation at the indicated time points (0, 1, 2 and 4 h); p53 and G3PDH mRNA expression was analysed by RT–PCR as described in the Materials and methods section. (**c**) Cells were analysed by immunofluorescence with the indicated antibodies (pAb421, DO-1 and monoclonal anti-p53ser15p antibody: 16G8) 12 h after Doxo stimulation. (**d**) Cells were collected 12 h after Doxo stimulation and subjected to cell fractionation experiments as described in Materials and methods. Twenty micrograms of the proteins extracted from the organelle was analysed by sodium dodecyl sulfate–polyacrylamide gel electrophoresis (SDS–PAGE)/western blot experiments using the indicated antibodies. Lamin was used as a positive control for nuclear localization, and β-tubulin for cytosolic localization.

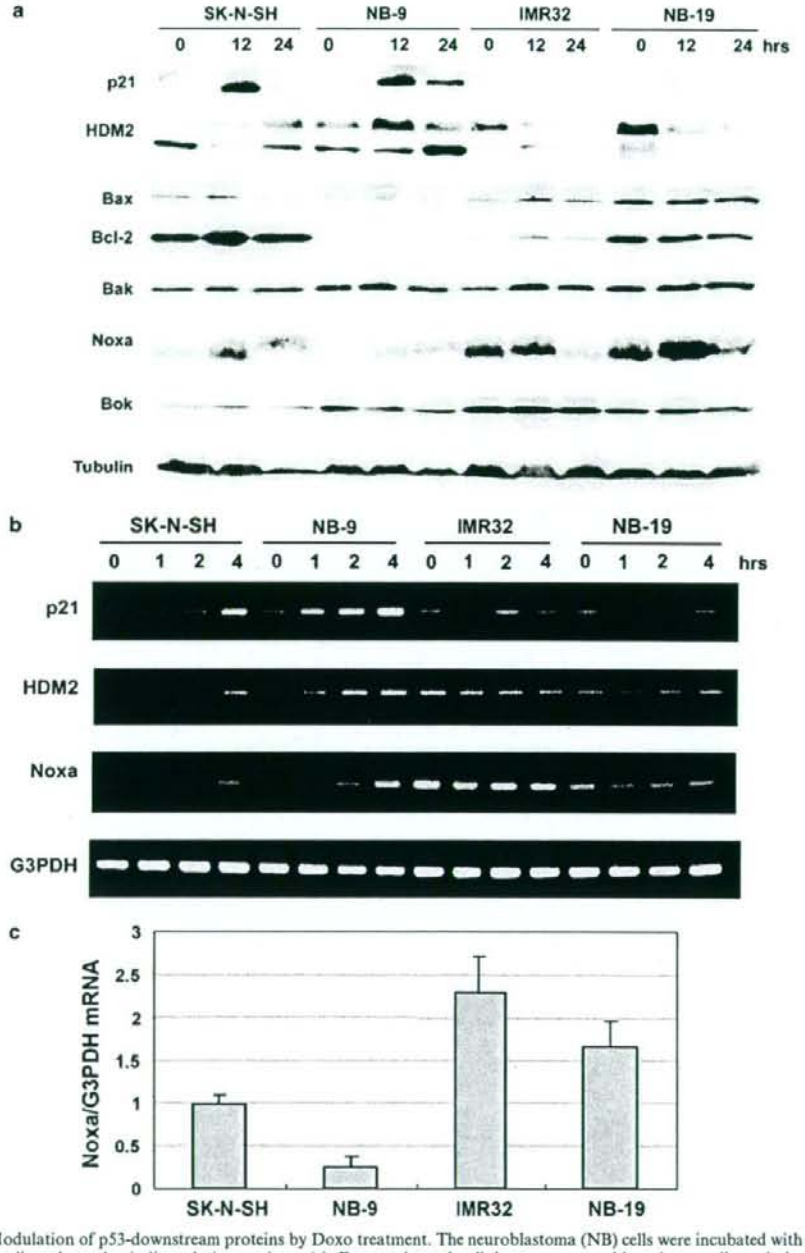

Figure 3 Modulation of p53-downstream proteins by Doxo treatment. The neuroblastoma (NB) cells were incubated with or without Doxo and collected at the indicated time points. **(a)** Extracted total cell lysates were subjected to sodium dodecyl sulfate–polyacrylamide gel electrophoresis (SDS–PAGE)/western blot analysis using the antibodies against the indicated molecules as described in Materials and methods. **(b)** Total RNA was subjected to semi-quantitative RT–PCR analysis as described in the Materials and methods section. **(c)** Quantitative real-time PCR analysis of *Noxa* mRNA amounts in NB cells as described in the methods section. Total RNA was extracted from unstimulated NB cells.

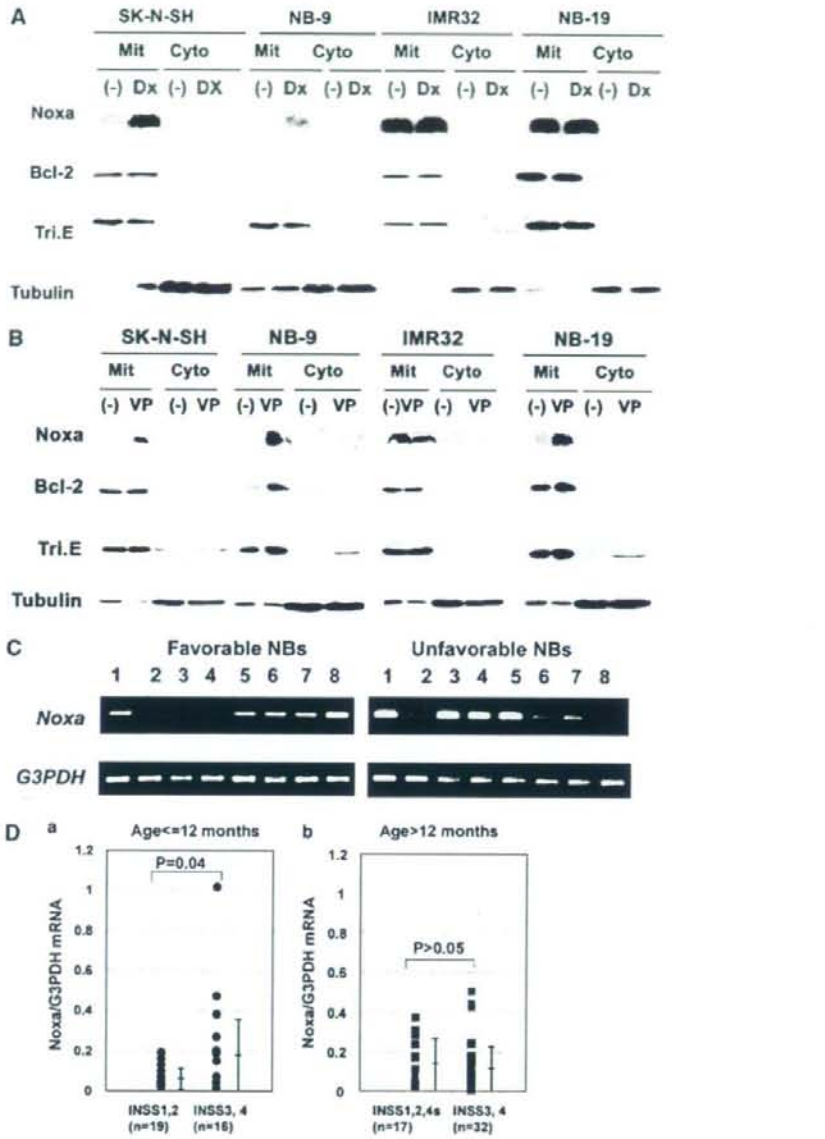

Figure 4 Noxa is upregulated in mitochondria by Doxo in the sensitive neuroblastoma (NB) cells. (**A** and **B**) Cells were collected 12 h after stimulation by Doxo (A, DX) or etoposide (B, VP) and subjected to cell fractionation for mitochondria (heavy membrane fraction: Mit) and the light membrane/cytosol fraction (Cyto). Samples were analysed by sodium dodecyl sulfate–polyacrylamide gel electrophoresis (SDS–PAGE)/western blotting with the indicated antibodies. Trifunctional protein (Tri E) and tubulin were controls for the mitochondrial fraction and cytosolic/light membrane fraction, respectively. This is a representative result of three independent experiments. (**C**) Semi-quantitative RT–PCR analysis of Noxa mRNA in favorable (stage 1 or 2, with single copy *MYCN*) and unfavorable (stage 3 or 4, with *MYCN* amplification) NB samples. (**D**) Quantitative real-time RT–PCR analysis of *Noxa* mRNA in 84 tumor samples from patients with NBs according to the tumor stage. The levels of Noxa were normalized to that of G3PDH. Results are presented as closed circles (**Da**) and closed squares (**Db**) with mean ± s.d. bars.